Original Article

Impact of Aortic Valve Leaflets Calcium Volume and Distribution on Post-TAVR Conduction Abnormalities

Author information:

Symon Reza[1], Brandon Kovarovic[1], and Danny Bluestein[1]

[1]Department of Biomedical Engineering, Stony Brook University, Stony Brook, New York, USA

Acknowledgment

The Dassault Systèmes SIMULIA Living Heart Project has provided the base framework of the 4-chamber beating heart model employed in this study as part of our academic collaboration with the company. The authors thank Dr. Matteo Bianchi for his contributions to the early stages of the project and for helping to develop the initial framework for analyzing CCAs in the beating heart, and Dr. Jiang Yao (Dassault Systèmes) for providing scientific insights.

Funding Source

This project was supported by the National Institutes of Health (NIH) through the National Institute of Biomedical Imaging and Bioengineering (NIBIB) under grant number U01EB026414 (DB).

***Corresponding author:**

Prof. Danny Bluestein

Department of Biomedical Engineering

Stony Brook University

Stony Brook, NY 11794-8084, USA

Tel: +1 (631) 444-2156

ORCID: 0000-0002-4014-2308

E-mail: danny.bluestein@stonybrook.edu

Abstract

Introduction: Transcatheter aortic valve replacement (TAVR) is increasingly used to treat aortic stenosis, including in low-risk patients. However, post-procedural cardiac conduction abnormalities (CCA), often requiring permanent pacemaker implantation (PPI), remain a concern. This study investigates how the volume and distribution of aortic leaflet calcium deposits influence the risk of post-TAVR CCA.

Methods: An electromechanically coupled four-chamber beating heart model was used to simulate TAVR with a self-expandable Evolut® 26 mm device. Five virtual patient scenarios were modeled with varying calcium volumes and distributions: no calcium, uniform distribution (3 Calc), and isolated calcification on the left coronary leaflet (LCL), right coronary leaflet (RCL), or non-coronary leaflet (NCL). Electrical conduction was simulated using a monodomain model and coupled with structural mechanics to evaluate tissue-device interactions. Metrics included principal stress, contact pressure, and contact pressure index (CPI) over three cardiac cycles.

Results: Larger calcium volumes and specific leaflet distributions increased stress and contact pressure near the atrioventricular node. The LCL model exhibited the highest mechanical stress and peak contact pressure (13.1 kPa), while the NCL model showed the lowest (6.42 kPa). The RCL model had intermediate values. Elevated contact pressure and stress in the LCL case suggest an increased risk of conduction disruption and PPI.

Conclusion: Leaflet calcium deposit volume and distribution significantly influence mechanical stress and contact dynamics near the conduction system following TAVR. These insights support the integration of clinical data, such as leaflet calcium volume and distribution into pre-procedural planning to personalize risk assessment and improve patient outcomes.

Keywords

TAVR, FEA, Conduction abnormality, PPI, Leaflet calcification, Living Heart Model

Acronyms

TAVR	Transcatheter aortic valve replacement
CCA	Cardiac conduction abnormality
MS	Membranous septum
PPI	Permanent pacemaker implantation
A-V	Atrioventricular
AOI	Area of interest
HB	His bundle
CPI	Contact pressure index
CTA	Computed tomography angiography
LBBB	Left bundle branch block
RBBB	Right bundle branch block
RCL	Right coronary leaflet
NCL	Non-coronary leaflet
LCL	Left coronary leaflet
ΔMSID	Subtraction of implantation depth from the membranous septum length

Highlights:

- Beating heart model used to assess post-TAVR conduction abnormality risk.
- Higher calcium volume increases contact pressure near conduction pathways.
- Left coronary leaflet calcification linked to elevated post-TAVR CCA risk.
- Dynamic simulations show stress fluctuations during cardiac cycles.
- Findings support personalized TAVR planning to reduce PPI need.

1. Introduction

Aortic stenosis has traditionally been treated with surgical aortic valve replacement (SAVR), while transcatheter aortic valve replacement (TAVR) has emerged as a minimally invasive alternative. With comparable hemodynamic outcomes, TAVR is now widely adopted in high- and intermediate-risk patients and has recently been approved for low-risk patients. However, this expansion raises concerns about complications such as paravalvular leakage, leaflet thrombosis, valve degeneration, and notably, cardiac conduction abnormalities (CCAs). Among these, CCAs are particularly persistent and often require permanent pacemaker implantation (PPI) [1-3], limiting TAVR's broader application. CCAs typically result from mechanical injury to the atrioventricular conduction system near the interleaflet triangle between the non-coronary and right coronary leaflets. PPI has been linked to increased mortality and heart failure hospitalizations [2, 4], making CCA risk prediction critical for improved pre-procedural planning.

Several clinical studies have identified risk factors for post-TAVR CCA, including preexisting right bundle branch block (RBBB), deeper implantation, short membranous septum length, low ΔMSID, and calcium burden. However, findings—especially on the volume and distribution of leaflet calcification—have been inconsistent. Some link high calcium on the left coronary leaflet (LCL) with increased PPI rates [5, 6], while others implicate the non-coronary (NCL) [7] or right coronary leaflets (RCL) [8]. These discrepancies complicate clinical decision-making and highlight the need for more precise predictive tools. Moreover, anatomical variability in the device landing zone limits the reliability of purely anatomical and procedural predictors. Since post-TAVR CCA depends on localized, dynamic interactions between the prosthesis and conduction fibers, computational modeling offers a promising way to enhance predictive accuracy.

Computational tools have been widely used to study TAVR complications like paravalvular leakage, thrombosis, and valve degeneration [9-14]. Patient-specific models have also been applied to analyze post-TAVR CCA risk, showing that elevated contact pressure or strain on the His bundle correlates with conduction damage [15-17]. Recently, we introduced a beating heart electro-mechanical model to simulate post-TAVR CCA risk under dynamic conditions [18]. While more physiologically accurate, this method is computationally demanding and not yet scalable to patient-specific workflows. However, it holds value in helping clinicians interpret how measurable parameters—such as calcium volume and distribution—affect post-TAVR outcomes and may reconcile inconsistent findings across clinical studies.

The Living Human Heart Model (**Error! Reference source not found.**a, b) is a high-fidelity, electromechanically coupled, four-chamber adult male heart developed under the SIMULIA Living Heart Project. It has been used to study various cardiovascular conditions and interventions, including TAVR, mitral repair, and LVADs [18-22]. Prior studies have mapped calcium patterns

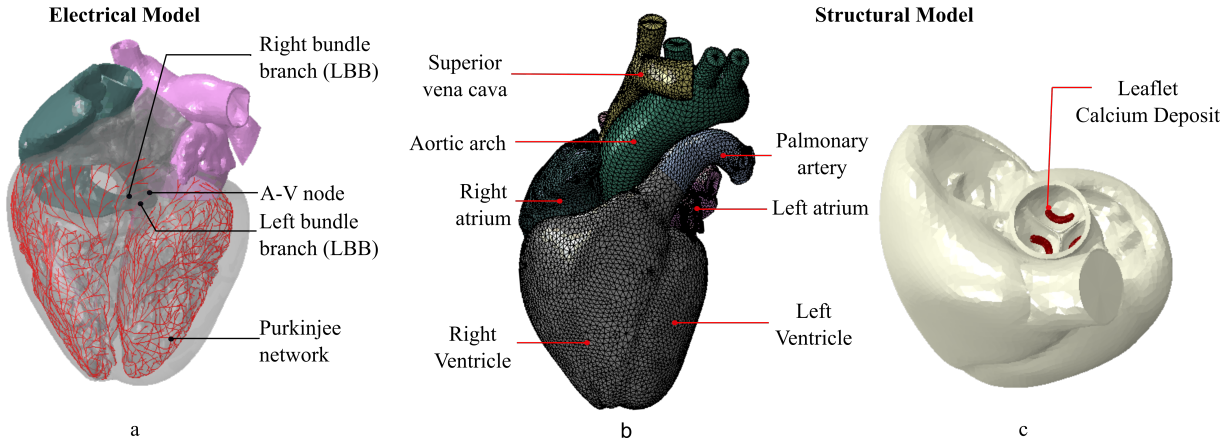

Figure 1: Illustration of the (a) electrical model, (b) finite element model, of the 4-chamber full heart model (Adapted with permission from Reza et al. Biomechanics and Modeling in Mechanobiology [18]), and (c) diseased heart with leaflet calcification.

on native leaflets [23] and Halevi et al. [24] used the reverse calcification technique (RCT) to

identify common geometries, showing deposits mainly along the coaptation line (**Error! Reference source not found.**), consistent with Thubrikar et al. [23].

In this study, we used the Living Human Heart Model to simulate common calcium distribution patterns by structurally modifying the native valve to introduce synthetic leaflet calcifications with varying volumes and distributions (**Error! Reference source not found.**c).Our goal was to evaluate their role in increasing CCA risk and provide insights that support clinically relevant, data-driven decision-making using readily available parameters such as calcium burden.

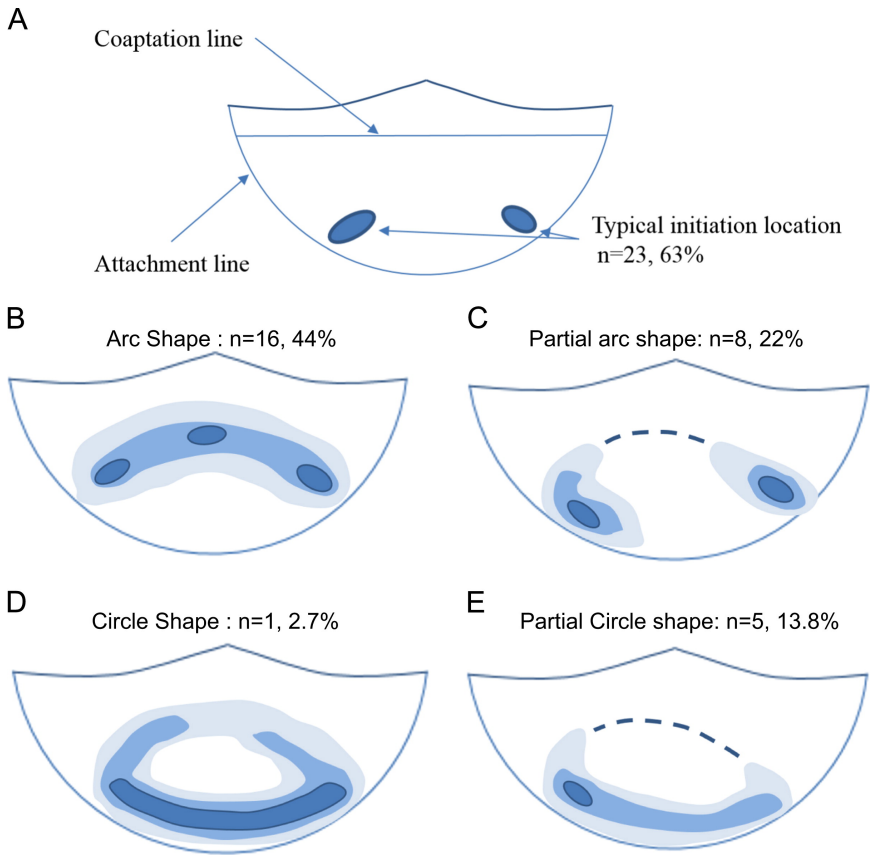

Figure 2: Common patterns of calcium deposits (Reproduced with permission from Halevi et al., Journal of Biomechanics [24])

2. Methods

A dynamic, high-fidelity four-chamber human heart model developed under the SIMULIA Living Heart Model [25], was used as the foundation for this study. This model employs a sequentially coupled electro-mechanical approach to simulate realistic cardiac function. Electrophysiological simulations of healthy cardiac conduction were performed first, and the resulting activation patterns were coupled with the structural model to replicate mechanical heart behavior. An Evolut® 26 mm TAVR device (Medtronic, Inc., Minneapolis, MN) was deployed within this beating heart model under five different aortic leaflet calcium deposit conditions. A 6 mm implantation depth—within the clinically recommended 3–6 mm range—was selected as the nominal case. The membranous septum (MS) length in the model was 5.5 mm, yielding ΔMSID values of -1.5 mm (aortic), +0.5 mm (nominal), and +2.5 mm (ventricular).

2.1. Calcium deposit model and distribution

To investigate how calcium volume and distribution affect post-TAVR CCA risk, we created parametric calcium deposit models based on commonly observed leaflet calcification shapes. Each

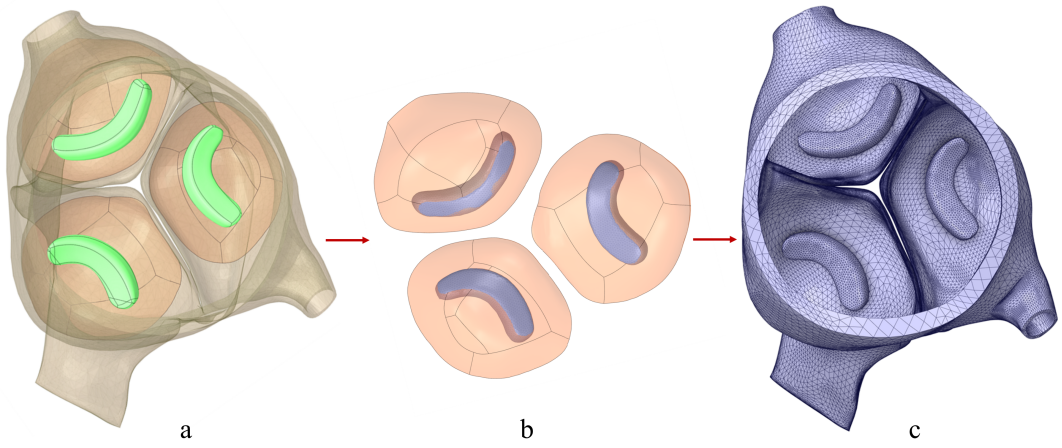

Figure 3: Idealized leaflet calcium deposit model creation, (a) CAD model creation, (b) leaflet surface fitting of the CAD models of the leaflet calcium deposits, and (c) meshed calcium deposit models.

leaflet-specific model was fitted to the Living Heart Model geometry with a average calcium volume of 85 mm^3. Five virtual patient scenarios were created (**Error! Reference source not found.**). : (1) a healthy case with no calcium deposits, (2) a case with uniform deposits across all three leaflets (3 Calc), and three cases with localized calcium on the non-coronary (NCL), right coronary (RCL), or left coronary (LCL) leaflet, respectively.

2.2. Modeling cardiac electrophysiology

Cardiac conduction was simulated in Abaqus/Standard using a monodomain reaction-diffusion model. Electrical signals propagated through both myocardial tissue and a 1D Purkinje fiber network, based on geometries from literature [25]. The model accounted for isotropic and anisotropic conduction and was solved using a staggered implicit Euler scheme over 500 ms of cardiac activity, beginning at 70% ventricular diastole. The heart was discretized into 297,635 tetrahedral elements, while the Purkinje network consisted of 10,757 1D elements, coupled to the myocardium through resistor-like conduction links. Electrical activation results were mapped to the mechanical model as boundary conditions, ensuring realistic electromechanical behavior. The implementation followed methods in the literature [26, 27].

2.3. Structural modeling

The structural model included detailed representations of both active and passive myocardial responses. Passive behavior followed an anisotropic hyperelastic formulation [29], with stiffness calibrated to match experimental strain data **[26]**. Active contraction was modeled using a time-varying elastance framework **[27]**, modulated by a contractility factor to replicate physiological ventricular twist and stroke volume. Fiber orientations ranged from -60° (epicardium) to +60° (endocardium) [28], capturing the heart's layered structure. Model calibration ensured accurate

ventricular deformation, chamber pressure-volume relationships, and realistic wall motion [29]. Further implementation details are available in the SIMULIA Living Heart Human Model User Guide (2018) [30].

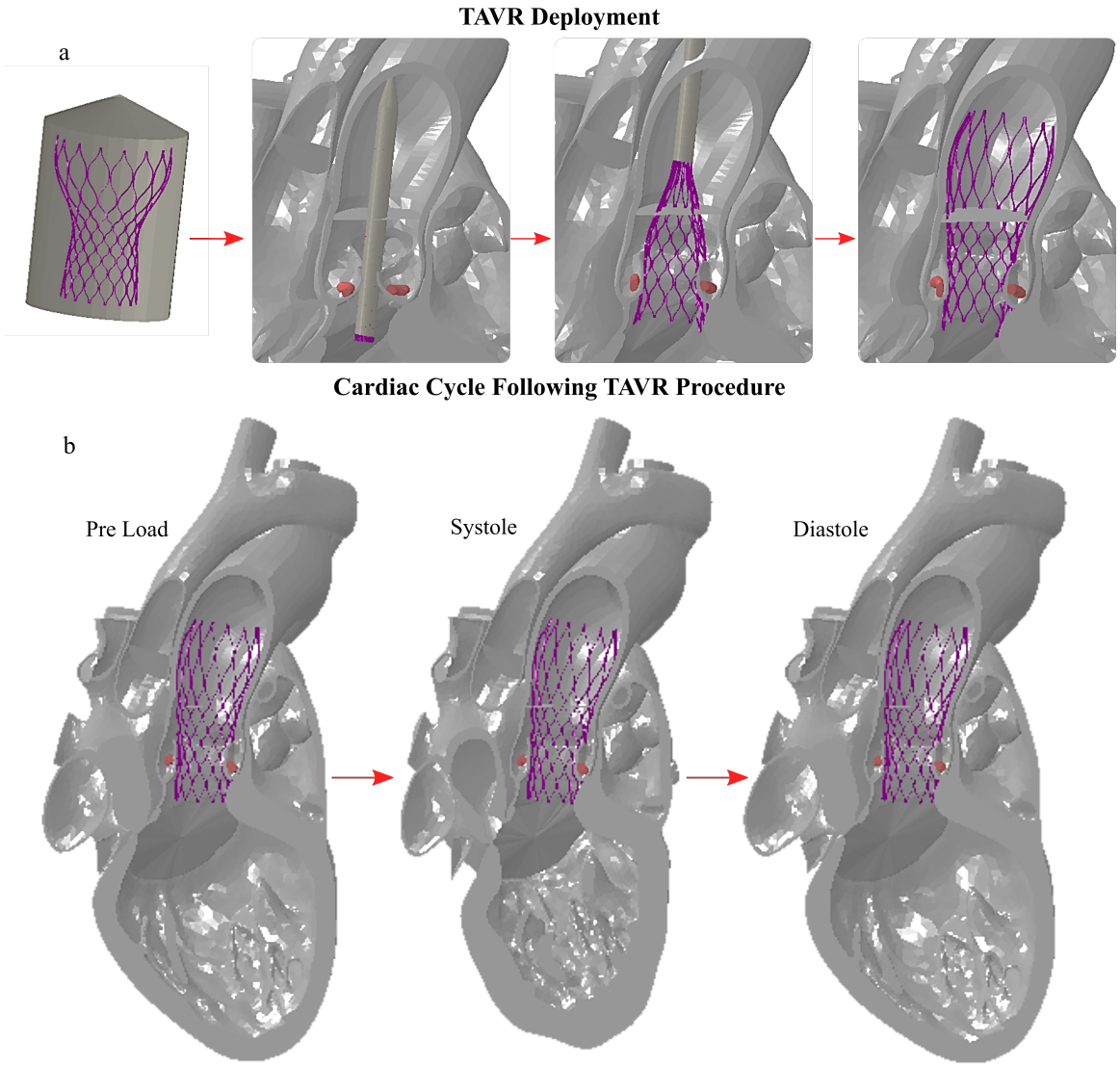

Figure 4: (a) TAVR implantation sequence from crimping to deployment, and (b) cardiac cycles following the procedure

2.4. Simulation parameters

The simulation was conducted in two stages: electrical and structural. In the first stage, cardiac conduction was simulated as described in Section 2.1. The resulting electrical activation data were applied as boundary conditions in the structural simulation to replicate realistic cardiac contraction using Abaqus Explicit 2019 (SIMULIA, Dassault Systèmes, Providence, RI). The structural phase included six sequential steps: crimping, placement, deployment, preload, beat, and recovery, spanning three cardiac cycles (Figure 4).

The TAVR stent was modeled using a structured hexahedral mesh and assigned a superelastic Nitinol material model [32, 33] , with further material details available in [17]. The His bundle (HB) is anatomically located between the atrioventricular membranous septum (MS) and the posterior crest of the muscular septum, beneath the interleaflet triangle between the non-coronary (NCL) and left-coronary (LCL) leaflets [34]. Accordingly, the area of interest (AOI) for stress and contact analysis was defined just below the MS, in the region between the NCL and LCL (**Error! Reference source not found.**), following the methodology outlined in Rocatello et al. [15].

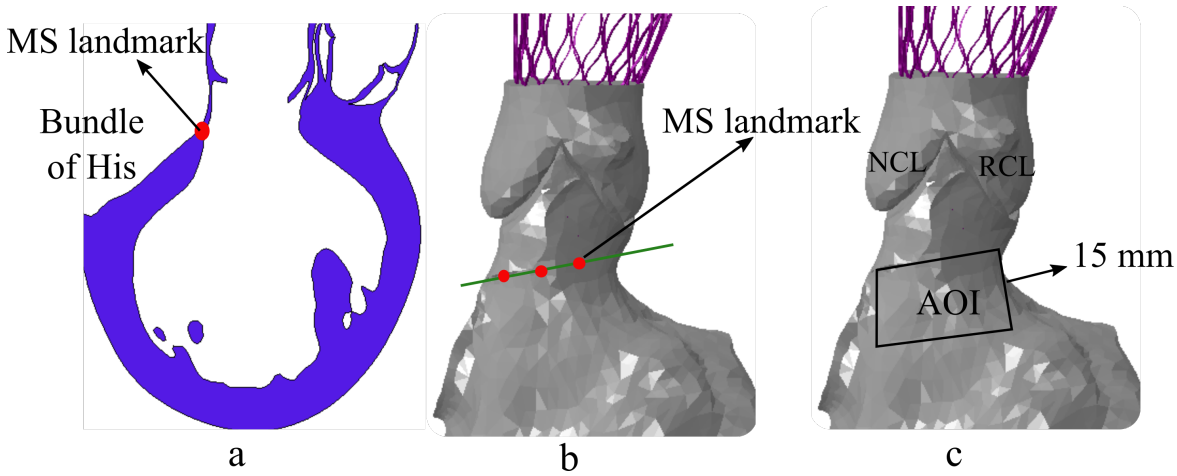

Figure 5: Illustration of the MS landmark from (a)) long axis view. Identified MS landmark in shown in green (b) and identified area of interest is confined to a black box (c).

3. Results

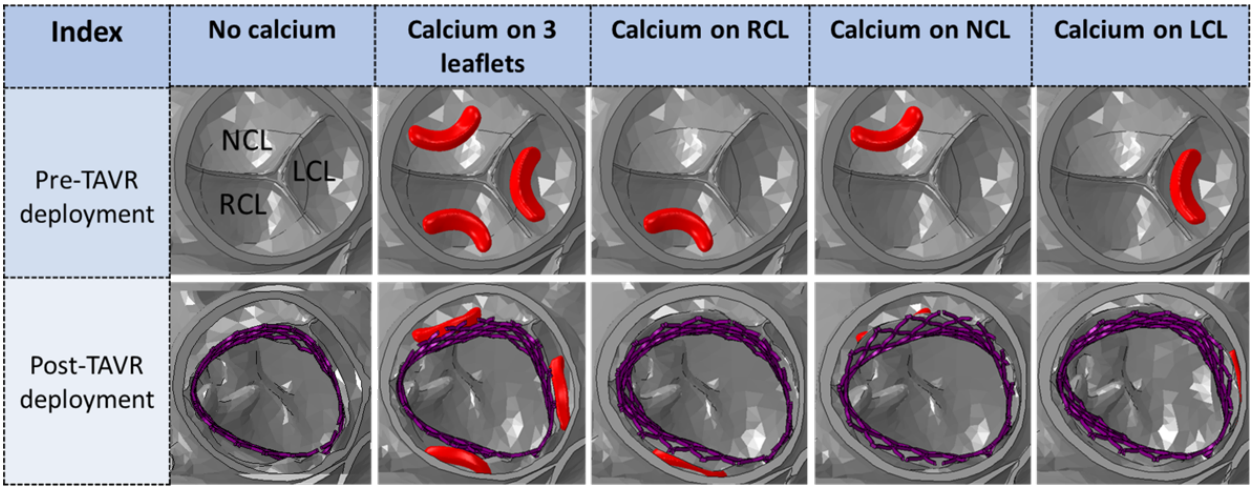

Figure 6: Pre-TAVR patient cases of various leaflet calcium deposit volume and distribution

The supra-annular Evolut® 26 mm device was implanted inside the aortic annulus of the modified Living Heart Model with five varying aortic leaflet calcium deposit volume and distribution (**Error! Reference source not found.**). To assess prosthesis–tissue interaction, three cardiac cycles were simulated following deployment. Hoop stresses on the area of interest (AOI) were evaluated for each case and compared to each other. Additionally, contact force, contact pressure, and the contact pressure index (CPI) were analyzed across all virtual patient scenarios.

3.1. Impact of calcium deposit volume

To evaluate the impact of calcium deposit volume on post-TAVR biomechanics, von Mises stress, principal stress components, and contact-based parameters—such as contact pressure and pressure index—on the area of interest (AOI) were analyzed. Following TAVR implantation, all three principal stress components increased. Over three cardiac cycles, the 3 Calc model showed stress increases of 20.95% (axial), 5.49% (radial), and 24.13% (hoop), while the No Calc model exhibited smaller increases of 16.52%, 7.19%, and 21.49%, respectively, compared to the healthy case.

Contact-based metrics also revealed substantial differences. During device deployment, maximum contact pressure peaked and stabilized by preload but fluctuated with each heartbeat post-deployment—reaching a peak from late systole to early diastole. The 3 Calc model experienced the highest contact pressure, peaking at 10.3 kPa with a mean of 1.93 kPa, while the No Calc model recorded a lower peak of 5.69 kPa and a mean of 0.52 kPa (**Error! Reference source not found.**a).

The cumulative contact pressure over three cardiac cycles was 234.61 kPa for the 3 Calc model and 65.88 kPa for the No Calc model (**Error! Reference source not found.**b).

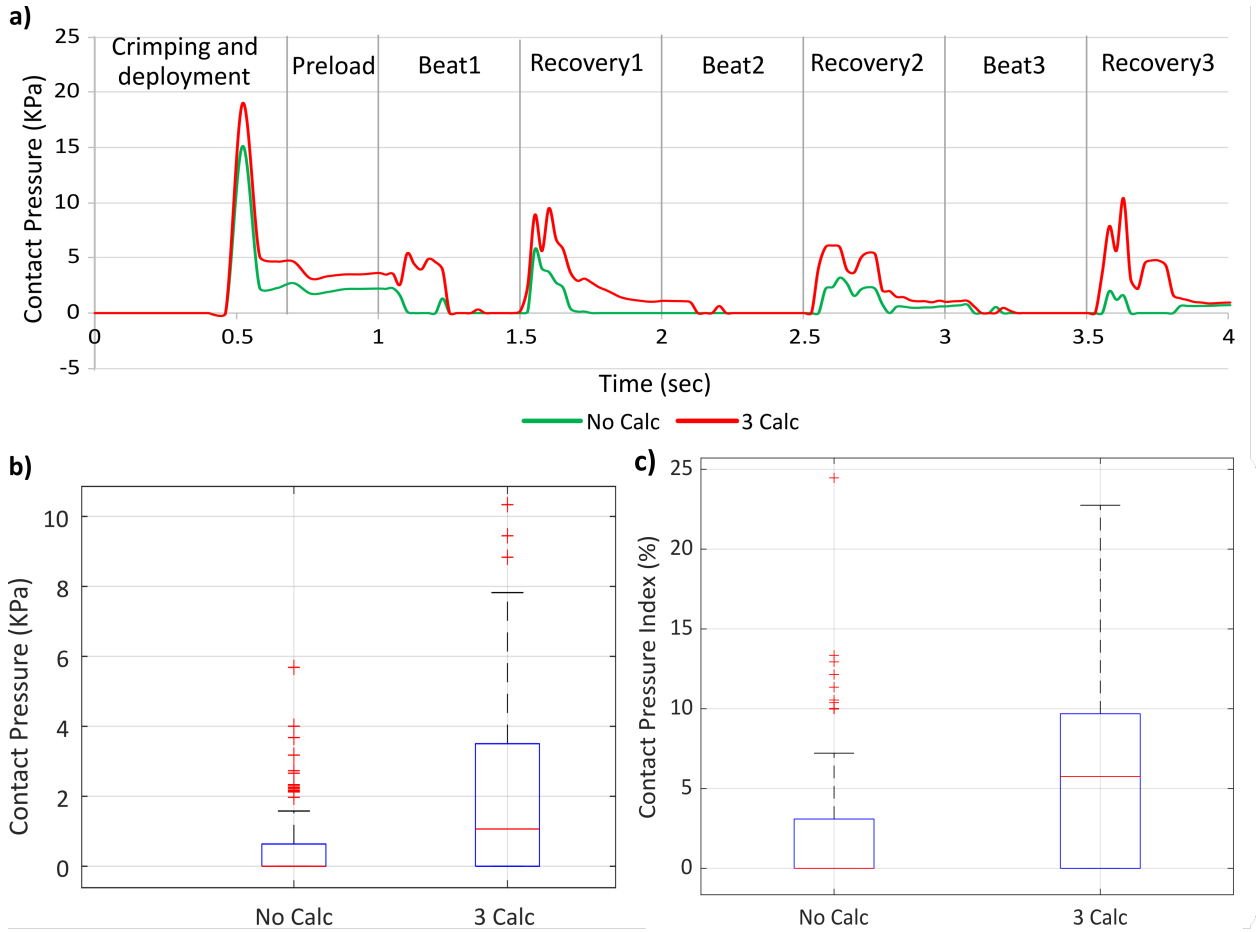

Figure 7: Effects of calcium deposit volume, (a) Contact pressure on the AOI at each step;(b) Box plots of contact pressure at the AOI across three cardiac cycles following TAVR implantation for two different calcium deposit volume, and (c) Contact Pressure Index (CPI) during the three cardiac cycles.. A Mann-Whitney U test comparing contact pressures across calcium deposit volume yielded a statistically significant difference ($P < 0.001$).

Additionally, contact area analysis revealed a slightly higher contact pressure index for the 3 Calc model (26.33%) compared to the No Calc model (25.2%) (**Error! Reference source not found.**c) , highlighting how increased calcium volume elevates mechanical stress and contact forces on the conduction system region.

3.2. Impact of calcium deposit distribution

A similar trend was observed with varying calcium deposit distributions. A pronounced peak in maximum contact pressure occurred during the TAVR deployment phase, stabilizing by the end

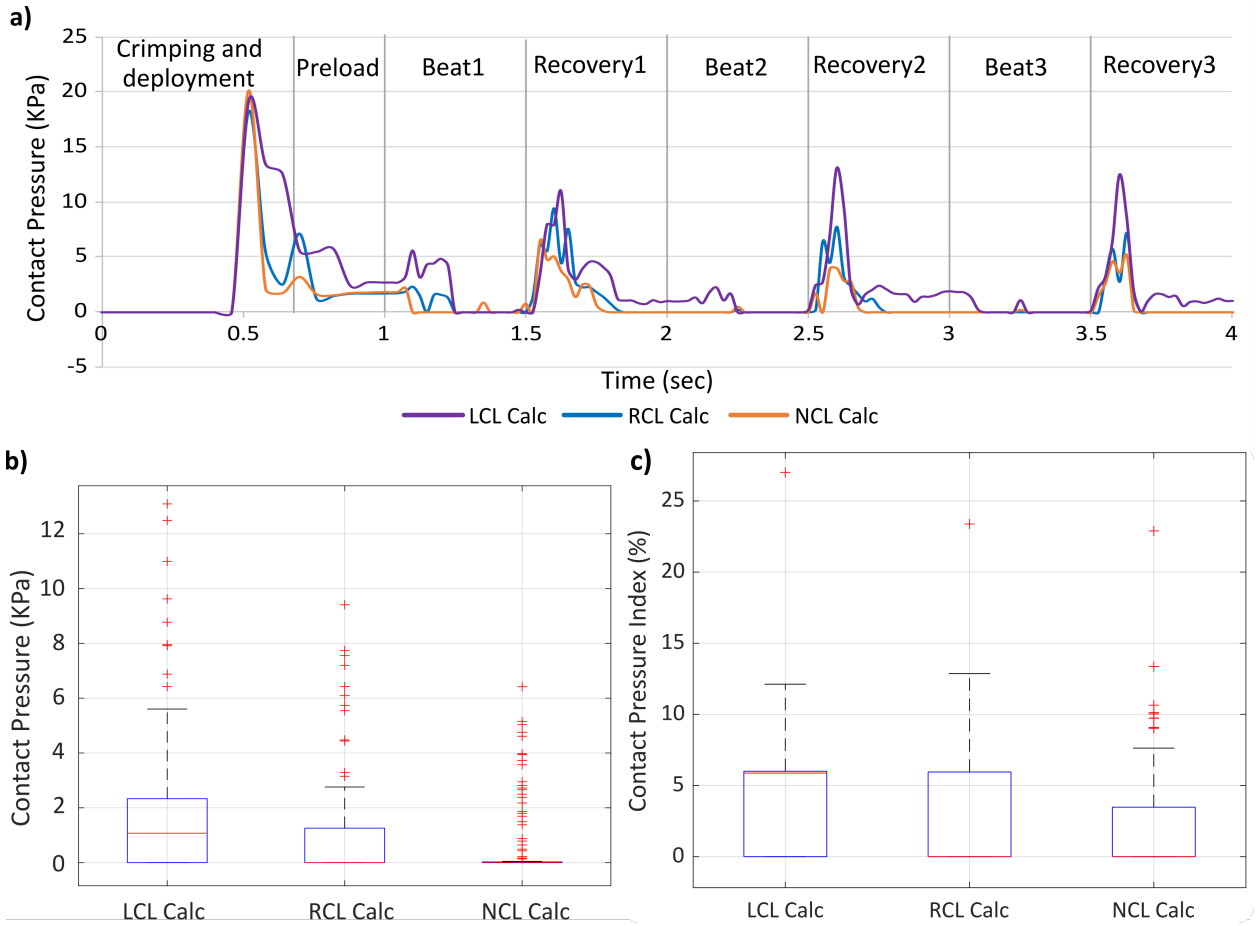

Figure 8: Effects of calcium deposit distribution, (a) Contact pressure on the AOI at each step, (b) Box plot diagrams of contact pressure at the AOI during three cardiac cycles following TAVR implantation for three distributions of calcium deposits, and (c) CPI during three cardiac cycles. Kruskal-Wallis test was performed between the contact pressures and contact pressure indexes three distributions of calcium deposits yielding P<0.001.

of deployment and preload. During subsequent heartbeats, contact pressure fluctuated cyclically, with peaks occurring from the late systole to early diastole in each cardiac cycle. The range of maximum principal stress components over three cardiac cycles was compared. The LCL Calc model showed increases of 15.96%, 8.38%, and 23% in axial, radial, and hoop stress, respectively. The RCL Calc model exhibited increases of 16.17%, 7.57%, and 22.64%, while the NCL Calc model showed smaller increases of 14.61%, 7.43%, and 19.42% in the same stress components.

Contact-based parameters also varied significantly. The LCL Calc model exhibited the highest contact pressure throughout the simulation, with a maximum of 13.1 kPa and a mean of 1.91 kPa. The RCL Calc model recorded a maximum of 9.41 kPa and a mean of 0.90 kPa, while the NCL Calc model had the lowest, with a peak of 6.42 kPa and a mean of 0.59 kPa (Figure 8a). The temporal sum of contact pressure across three cardiac cycles further reflected these differences, with values of 232.40 kPa for LCL, 110.72 kPa for RCL, and 73.24 kPa for NCL (Figure 8b). Contact area analysis showed contact pressure indices of 25.67%, 20%, and 25.80% for the LCL, RCL, and NCL Calc models, respectively (Figure 8c), highlighting how both calcium distribution and leaflet location influence prosthesis–tissue interaction.

4. Discussion

Post-TAVR cardiac conduction abnormalities (CCA) remain a critical complication, often leading to permanent pacemaker implantation (PPI). PPI is associated with increased mortality and heart failure hospitalizations, impacting the broader success of TAVR. This complication underscores the critical need of identifying and understanding the anatomical and procedural factors contributing to post-TAVR CCA. Key contributors to these conduction abnormalities include prosthesis implantation depth, membranous septum (MS) length, (ΔMSID), preexisting RBBB, and calcium burden. Understanding the complex interplay between post-procedural CCA,

193 preexisting conduction abnormalities, and the interaction between the TAVR prosthesis and
194 cardiac conduction fibers remain a challenge. Previously, we introduced an innovative approach
195 using a high-fidelity, electro-mechanically coupled beating heart model, which provided deeper
196 insights into the relationship between these abnormalities and factors such as implantation depth
197 and preexisting cardiac asynchronies [18]. However, that study was limited to parametric
198 modeling. Furthermore, clinical studies sought to establish a link between commonly accessible
199 clinical data, such as the volume and distribution of calcium deposits on the aortic leaflets, and the
200 new onset of post-TAVR CCA, but the findings were inconclusive, prompting us to numerically
201 investigate how the volume and distribution of aortic leaflet calcium deposits influence the onset
202 of CCA. Accordingly, in this study, we parametrically modified the model to evaluate the relative
203 risk of post-TAVR CCA based on the volume and distribution of leaflet calcium deposits.

204 The results of this study show that both the volume and distribution of aortic leaflet calcium
205 deposits significantly influence the risk of post-TAVR CCA. When calcium is concentrated on
206 certain leaflets, it alters prosthesis expansion, increasing contact pressure and mechanical stress
207 within the area of interest (AOI) throughout the cardiac cycle. This observation is consistent with
208 prior research suggesting that high volume of calcification may contribute to mechanical damage
209 to the conduction system and increase the relative risk of post TAVR CCA [8, 31-33]. Specifically,
210 LCL calcification led to the highest stress and pressure within the AOI, as the device was deflected
211 toward the RCL–NCL junction. This suggests that calcification on the LCL may heighten the risk
212 of post-TAVR CCA, particularly for self-expandable TAVR procedures. Conversely, calcium
213 deposits on the RCL led to lower stress and contact pressure than in the LCL Calc model yet
214 remained significantly higher than those in the NCL Calc model.

Additionally, the curvature of the aortic arch pushes the top crown of the Evolut® device toward the LCL, causing the calcified leaflets to act as a pivotal plane. This leads to rotational forces twisting the bottom crown, shifting it towards the opposite direction- approximately toward the AOI, while larger deposits on the NCL slightly shift the prosthesis toward the RCL, shielding the AOI from contact with the prosthesis. It is important to note that the study used a parametric model for calcium deposits, whereas in reality, the shape of calcium deposits tends to be uneven. This suggests that similar calcium distributions with varying shapes could yield different outcomes. Therefore, patient-specific modeling may further increase the accuracy for assessing the risk of post-TAVR CCA.

Previous clinical studies have investigated leaflet calcium distribution as a predictor of post-TAVR CCA and the need for PPI. Many of these studies focused on either balloon-expandable devices or both balloon- and self-expandable devices. For example, Mauri et al. [34] and Bianchini et al. [8] examined balloon-expandable devices and found that a higher calcium volume at the left ventricular outflow tract (LVOT) below the LCL and RCL, respectively, was associated with an increased need for PPI. Fujita et al. [5] studied both balloon- and self-expandable devices and identified high calcium distribution on LCL as a contributing factor to the need for PPI. In contrast, Pollari et. al. [35] and Gama et. al. [36] found calcium deposits below the NCL at the LVOT to be linked with the need for PPI. Veulemans et al. [6] and Sharma et. al. [7] focused on self-expandable TAVR systems and identified high calcification on the LCL as a dependent variable. The current study observed that higher calcium volumes in the LCL increase the risk of post-TAVR CCA which aligned with the observation from Veulemans et al. [6] and Sharma et. al. [7] both of the studies focusing on self-expandable devices. These findings suggest that mixing balloon-expandable and self-expandable devices in studies could yield conflicting

results, and leaflet calcification may not be a uniform risk factor across device types, as the material properties, shapes, and implantation techniques of these devices differ significantly. Furthermore, well-established anatomical and procedural factors such as implantation depth, membranous septum length (ΔMSID), and preexisting RBBB are likely to play a central role in post-TAVR outcomes, while leaflet calcium volume and distribution may act as secondary risk enhancers rather than primary drivers.

In summary, this study aimed to clarify the conflicting clinical findings on the relationship between specific calcification patterns and the need for post-procedural pacemaker implantation (PPI). By closely examining the interaction between the TAVR device and the AOI across varying calcium deposit volumes and distributions—while keeping other anatomical and procedural parameters constant, the study provides valuable insights into this complex association. The results indicated that the volume of calcium deposits on the aortic leaflets may increase the risk of post TAVR CCA in self-expandable TAVR devices. High calcium deposit volume on the LCL may increase the risk compared to RCL and NCL for self-expandable TAVR devices. Calcium deposits on the LVOT and balloon expandable devices need to be studied separately to understand the device type specific effect of calcium deposits on the onset of CCA and the need for PPI.

The dynamic fluctuations in contact pressure throughout the cardiac cycle emphasize the need to account not only for static anatomical features but also for the complex dynamic biomechanical interactions between the TAVR prosthesis and surrounding cardiac structures during the entire cardiac cycle. Particularly, variations in contact pressure during the transition from late systole to early diastole may indicate transient mechanical stresses that increase the likelihood of the new onset of CCA following TAVR procedures. While traditional clinical parameters are essential, the integration of anatomical features and high-fidelity simulations allows

for a more nuanced understanding of the biomechanical interactions that underlie post-TAVR complications. This approach could lead to more personalized pre-procedural planning, potentially reducing the incidence of CCA and improving overall patient outcomes. Overall, the findings suggest that clinicians should consider both volume and spatial pattern of calcium, especially on the LCL, when using Nitinol-based, supra-annular TAVR devices. These insights may improve risk stratification and guide personalized TAVR strategies.

5. Limitations

This study used idealized calcium shapes and average volumes to assess post-TAVR CCA risk. While this enabled controlled comparisons, incorporating patient-specific calcium geometries would improve clinical applicability. Simulations employed a unidirectional electro-mechanical coupling using the Living Human Heart Model (LHHM), excluding mechano-electrical feedback. Prior research indicates this omission has a minimal impact on conduction velocity [37] supporting the model's validity for this application. The use of a standard healthy male heart model provides consistency but may not reflect anatomical variability in typical TAVR patients. Adapting simulations to patient-specific heart models will allow more accurate identification of mechanical thresholds linked to CCA risk. We plan to expand our current simulations to incorporate patient-specific models.

6. Conclusions

This study investigated how the volume and distribution of leaflet calcifications influence the risk of developing post-TAVR cardiac conduction abnormalities (CCA) that may necessitate a permanent pacemaker implantation (PPI). By evaluating the interaction between the TAVR device and the area of interest (AOI) under varying calcium patterns—while controlling for other

anatomical and procedural variables, the results suggest that increased leaflet calcium burden, particularly on the left coronary leaflet (LCL), elevates CCA risk in self-expandable devices.

This study used of a beating heart model that captures the dynamic interplay between the device, tissue, and calcifications, offering a more physiologically realistic assessment compared to static device implantation analysis. This method supports personalized pre-procedural planning and can guide the design of next-generation TAVR devices aimed at reducing CCA risk and improving patient outcomes.

Acknowledgment

The Dassault Systèmes SIMULIA Living Heart Project has provided the base framework of the 4-chamber beating heart model employed in this study as part of our academic collaboration with the company. The authors thank Dr. Matteo Bianchi for his contributions to the early stages of the project and for helping to develop the initial framework for analyzing CCAs in the beating heart, and Dr. Jiang Yao (Dassault Systèmes) for providing scientific insights.

Funding Source

This project was supported by the National Institutes of Health (NIH) through the National Institute of Biomedical Imaging and Bioengineering (NIBIB) under grant number U01EB026414 (DB).

Reference:

1. Boonyakiatwattana, W., et al., *Preprocedural and procedural variables that predict new-onset conduction disturbances after transcatheter aortic valve replacement.* BMC Cardiovasc Disord, 2022. **22**(1): p. 135.
2. Faroux, L., et al., *Clinical impact of conduction disturbances in transcatheter aortic valve replacement recipients: a systematic review and meta-analysis.* Eur Heart J, 2020. **41**(29): p. 2771-2781.
3. Jorgensen, T.H., et al., *Mortality and Heart Failure Hospitalization in Patients With Conduction Abnormalities After Transcatheter Aortic Valve Replacement.* JACC Cardiovasc Interv, 2019. **12**(1): p. 52-61.

4. Jørgensen, T.H., et al., *Mortality and heart failure hospitalization in patients with conduction abnormalities after transcatheter aortic valve replacement.* JACC: Cardiovascular Interventions, 2019. **12**(1): p. 52-61.
5. Fujita, B., et al., *Calcium distribution patterns of the aortic valve as a risk factor for the need of permanent pacemaker implantation after transcatheter aortic valve implantation.* European Heart Journal - Cardiovascular Imaging, 2016.
6. Veulemans, V., et al., *New insights on potential permanent pacemaker predictors in TAVR using the largest self-expandable device.* Cardiovascular diagnosis and therapy, 2020. **10**(6): p. 1816.
7. Sharma, E., et al., *Aortic valve calcification as a predictor of post-transcatheter aortic valve replacement pacemaker dependence.* Cardiology Research, 2020. **11**(3): p. 155.
8. Bianchini, F., et al., *Anatomical Annulus Predictors of New Permanent Pacemaker Implantation Risk after Balloon-expandable Trans-catheter Aortic Valve Implantation.* The American Journal of Cardiology, 2024.
9. Anam, S.B., et al., *Assessment of paravalvular leak severity and thrombogenic potential in transcatheter bicuspid aortic valve replacements using patient-specific computational modeling.* Journal of Cardiovascular Translational Research, 2021: p. 1-11.
10. Bianchi, M., et al., *Patient-specific simulation of transcatheter aortic valve replacement: impact of deployment options on paravalvular leakage.* Biomech Model Mechanobiol, 2019. **18**(2): p. 435-451.
11. Fumagalli, I., et al., *Fluid-structure interaction analysis of transcatheter aortic valve implantation.* International Journal for Numerical Methods in Biomedical Engineering, 2023. **39**(6): p. e3704.
12. Kovarovic, B.J., et al., *Mild Paravalvular Leak May Pose an Increased Thrombogenic Risk in Transcatheter Aortic Valve Replacement (TAVR) Patients-Insights from Patient Specific In Vitro and In Silico Studies.* Bioengineering, 2023. **10**(2): p. 188.
13. Oks, D., et al., *Effect of Sinotubular Junction Size on TAVR Leaflet Thrombosis: A Fluid–Structure Interaction Analysis.* Annals of Biomedical Engineering, 2023: p. 1-15.
14. Oks, D., et al., *Fluid-structure interaction analysis of eccentricity and leaflet rigidity on thrombosis biomarkers in bioprosthetic aortic valve replacements.* bioRxiv, 2022.
15. Bosi, G.M., et al., *A validated computational framework to predict outcomes in TAVI.* Scientific reports, 2020. **10**(1): p. 1-11.
16. Rocatello, G., et al., *Patient-specific computer simulation to elucidate the role of contact pressure in the development of new conduction abnormalities after catheter-based implantation of a self-expanding aortic valve.* Circulation: Cardiovascular Interventions, 2018. **11**(2): p. e005344.
17. Reza, S., et al., *A computational framework for post-TAVR cardiac conduction abnormality (CCA) risk assessment in patient-specific anatomy.* Artificial Organs, 2022.
18. Reza, S., B. Kovarovic, and D. Bluestein, *Assessing post-TAVR cardiac conduction abnormalities risk using an electromechanically coupled beating heart.* Biomechanics and Modeling in Mechanobiology, 2024: p. 1-17.
19. Galili, L., A. White Zeira, and G. Marom, *Numerical biomechanics modelling of indirect mitral annuloplasty treatments for functional mitral regurgitation.* Royal Society Open Science, 2022. **9**(1): p. 211464.

20. Ghosh, R.P., et al., *Numerical evaluation of transcatheter aortic valve performance during heart beating and its post-deployment fluid-structure interaction analysis.* Biomech Model Mechanobiol, 2020. **19**(5): p. 1725-1740.
21. Heidari, A., et al., *Patient-specific finite element analysis of heart failure and the impact of surgical intervention in pulmonary hypertension secondary to mitral valve disease.* Medical biological engineering computing, 2022. **60**(6): p. 1723-1744.
22. Pasta, S., et al., *Numerical simulation of transcatheter mitral valve replacement: The dynamic implication of LVOT obstruction in the valve-in-ring case.* Journal of Biomechanics, 2022. **144**: p. 111337.
23. Thubrikar, M.J., J. Aouad, and S.P. Nolan, *Patterns of calcific deposits in operatively excised stenotic or purely regurgitant aortic valves and their relation to mechanical stress.* The American journal of cardiology, 1986. **58**(3): p. 304-308.
24. Halevi, R., et al., *Progressive aortic valve calcification: Three-dimensional visualization and biomechanical analysis.* Journal of Biomechanics, 2014(0).
25. Baillargeon, B., et al., *The living heart project: a robust and integrative simulator for human heart function.* European Journal of Mechanics-A/Solids, 2014. **48**: p. 38-47.
26. Genet, M., et al., *Modeling pathologies of diastolic and systolic heart failure.* Annals of biomedical engineering, 2016. **44**: p. 112-127.
27. Walker, J.C., et al., *MRI-based finite-element analysis of left ventricular aneurysm.* American Journal of Physiology-Heart Circulatory Physiology, 2005. **289**(2): p. H692-H700.
28. Streeter Jr, D.D., et al., *Fiber orientation in the canine left ventricle during diastole and systole.* Circulation research, 1969. **24**(3): p. 339-347.
29. Sack, K.L., et al., *Construction and validation of subject-specific biventricular finite-element models of healthy and failing swine hearts from high-resolution DT-MRI.* Frontiers in Physiology, 2018. **9**: p. 539.
30. *SIMULIA Living Heart Human Model User Guide*. LHHM 2.1 Beta Release. 2018, United States: Dassault Systèmes Simulia Corp.
31. Gonska, B., et al., *Predictors for permanent pacemaker implantation in patients undergoing transfemoral aortic valve implantation with the Edwards Sapien 3 valve.* Clinical Research in Cardiology, 2017. **106**: p. 590-597.
32. Kaneko, H., et al., *Predictors of permanent pacemaker implantation after transcatheter aortic valve implantation for aortic stenosis using Medtronic new generation self-expanding CoreValve Evolut R.* Heart Vessels, 2019. **34**(2): p. 360-367.
33. Maeno, Y., et al., *A highly predictive risk model for pacemaker implantation after TAVR.* JACC: Cardiovascular Imaging, 2017. **10**(10 Part A): p. 1139-1147.
34. Mauri, V., et al., *Predictors of permanent pacemaker implantation after transcatheter aortic valve replacement with the SAPIEN 3.* JACC: Cardiovascular Interventions, 2016. **9**(21): p. 2200-2209.
35. Pollari, F., et al., *Risk factors for atrioventricular block after transcatheter aortic valve implantation: a single-centre analysis including assessment of aortic calcifications and follow-up.* EP Europace, 2019. **21**(5): p. 787-795.
36. Gama, F., et al., *Predictors of pacemaker implantation after TAVI in a registry including self, balloon and mechanical expandable valves.* The International Journal of Cardiovascular Imaging, 2022. **38**(1): p. 225-235.

37. Costabal, F.S., et al., *The importance of mechano-electrical feedback and inertia in cardiac electromechanics.* Computer Methods in Applied Mechanics and Engineering, 2017. **320**: p. 352-368.